frontiers | Frontiers in Earth Science

TYPE Original Research
PUBLISHED 21 September 2022
DOI 10.3389/feart.2022.986942

OPEN ACCESS

EDITED BY
Jingyu Wang,
Nanyang Technological University, Singapore

REVIEWED BY
Yi Fan,
Nanjing University of Information Science and Technology, China
Anning Huang,
Nanjing University, China

*CORRESPONDENCE
Jianqi Zhang,
pla1990@yeah.net

SPECIALTY SECTION
This article was submitted to Atmospheric Science, a section of the journal Frontiers in Earth Science

RECEIVED 05 July 2022
ACCEPTED 18 August 2022
PUBLISHED 21 September 2022

CITATION
Chen C, Zhang J and Chen X (2022), Response of North Pacific storm tracks to multiscale SST anomalies in a stable state of the Kuroshio extension system during the cold season.
Front. Earth Sci. 10:986942.
doi: 10.3389/feart.2022.986942

Response of North Pacific storm tracks to multiscale SST anomalies in a stable state of the Kuroshio extension system during the cold season

Chaohui Chen, Jianqi Zhang* and Xiangguo Chen

College of Meteorology and Oceanography, National University of Defense Technology, Changsha, Hunan, China

In the present study, the response of North Pacific storm tracks to spatial multiscale (large-scale and mesoscale) sea surface temperature anomalies (SSTAs) in stable state of Kuroshio Extension (KE-related SSTAs) system are investigated. The results show that storm tracks are significantly strengthened with local enhanced rainfall in the central North Pacific and near the west coast of the North American continent in response to KE-related large-scale SSTAs, while they shift to the north and are significantly strengthened in the central-eastern North Pacific and Gulf of Alaska with remote impact on precipitation along west coast of North America continent in response to KE-related mesoscale SSTAs. The anomalous storm tracks influenced by KE-related SSTAs at different spatial scales are closely related to the locations of low-level baroclinicity. The response of horizontal advection of temperature to different scales of KE-related SSTAs in the lower atmosphere plays an important role in resulting baroclinicity anomalies.

KEYWORDS

Kuroshio Extension, multiscale SSTAs, baroclinicity, storm tracks, atmospheric circulation

Introduction

The Kuroshio Extension (KE) system is characterized by pronounced variations between stable and unstable states (Qiu et al., 2014). In the stable state, the KE jet is strengthened and shifts northward, with weakened regional mesoscale eddy activity and an intensified southern recirculation gyre. The opposite occurs in the unstable state. Variations of KE accompanying multiscale sea surface temperature anomalies (SSTAs) can often affect the storm tracks, and especially KE-related mesoscale SSTAs are still understudied but remain very important for storm track variability.

Previous work indicates that decadal fluctuations of the KE large-scale dynamic state are the primary cause of local SST changes (Qiu 2000; Vivier et al., 2002), which strongly affects the air–sea heat flux exchange over the KE region (Tanimoto et al., 2003; Wang and Liu, 2015). This heat flux plays an important role in maintaining surface baroclinicity,

which both anchors and energizes storm tracks (Nakamura et al., 2004). Therefore, changes in the KE dynamic state may exert a significant impact on the North Pacific storm tracks. Révelard et al. (2016, 2018) found that in the stable state of KE system, the storm track activity in the northeast Pacific Ocean and Alaska is significantly strengthened. Qiu et al. (2014) indicated that changes in the KE state can result in large-scale uniform warming or cooling over the western and central North Pacific (see their Figure 6A) and can alter the position of storm tracks. However, the KE is also a region with abundant mesoscale features, including the oceanic front (Chen and Zurita-Gotor, 2008; Kida et al., 2015) and eddies (Qiu and Chen, 2005; Qiu and Chen 2010). Therefore, changes in the dynamic state of KE also expected to be manifest in mesoscale SSTAs. Wang and Liu (2015) determined that KE-related mesoscale SSTAs are aligned zonally and collocate with the troughs and ridges of KE meanders. Mesoscale KE SSTAs can also induce pronounced changes in storm tracks, and the change in the storm track anomaly is influenced by both mesoscale ocean front and mesoscale ocean eddy. The oceanic baroclinic adjustment proposed by Nakamura et al. (2008) suggests that the near-surface baroclinicity is sustained by a cross-frontal sensible heat flux, contributing to the intensity of a storm track. Taguchi et al. (2009) found that the weakening of KE fronts would weaken the low-level storm track and shift it to the south. The meridional shift of the KE oceanic front significantly modulates the intensity of the storm tracks (Kwon and Joyce. 2013). Using an idealized model, Foussard et al.(2018) indicated the meridional shift of the storm track following the oceanic fronts. As mentioned above, in addition to a mesoscale ocean front, a mesoscale ocean eddy can also affect the storm track anomaly (Ma et al., 2015). Ma et al. (2017) showed that the mesoscale SSTA variability in the KE could enhance storm tracks over north-eastern Pacific, and the intensity of storm track would decrease 15% after removing the mesoscale KE SSTA. Zhang et al. (2020) conducted similar experiments to those of Ma et al. (2015) using an AGCM and found the low level storm track decreased by about 20%.

In other numerical experiments, randomly adding some mesoscale SSTA disturbances can make the westerly jet shift northward with a northward-strengthened storm track (Foussard et al., 2018; Sun et al., 2018); these mesoscale SSTAs usually affect the storm track by enhancing baroclinicity and latent heat in the lower atmosphere. Due to the nonlinear nature of the Clapeyron-Clausius function, the positive and negative diabatic heating associated with warm eddies and cold eddies cannot cancel each other, which leads to positive net water vapor flux and diabatic heating after adding cold eddies and warm eddies randomly. The ensemble numerical experiment in Zhang et al. (2021) mainly investigated the feedback effects of mesoscale SSTAs and large-scale warming SSTAs on large-scale low-frequency atmospheric circulation. It was found that mesoscale SSTAs could strengthen the westerly jet with a shift to northward, and at the same time, mesoscale SSTAs could stimulate a remarkable counterclockwise circulation, similar to a Ferrell cell. Diagnostics show that the feedback of synoptic transient eddy stimulated by mesoscale SSTAs are the largest reason for low-frequency atmospheric circulation anomaly, but the accompanying diabatic heating was weak. However, under the influence of large-scale warming SSTAs, diabatic heating is stronger and can stimulate a significant clockwise secondary circulation in the altitude-latitude section. Diagnostic analysis shows that diabatic heating is the main factor affecting large-scale low-frequency circulation in the central North Pacific.

From the above, KE-related SSTAs present obvious multispatial scale characteristics, and all of them have significant impacts on storm track anomalies. Because storm tracks are important factors that modulate the atmospheric response to mid-latitude SSTAs (Peng and Whitaker 1999; Kushnir et al., 2002; Taguchi et al., 2012; Okajima et al., 2018; Zhang et al., 2021), clarifying the impacts of KE-related multiscale SSTAs, especially KE-related mesoscale SSTAs, on storm tracks is critical to deepening our understanding of the climatological effects of the KE system. Therefore, our objective is to highlight the differential responses of North Pacific storm tracks to the large-scale and mesoscale SSTAs in the KE. We use ensemble numerical experiments to diagnose the fundamental mechanisms involving this air-sea interaction (Zhang et al., 2021). The remainder of this article is organized as follows: The datasets and methods used in this study are briefly introduced in the next section. The following section evaluates the performance of model on storm tracks. After this, the next section investigates the response of storm tracks to large-scale and mesoscale SSTAs induced by KE dynamic state. The possible reasons for the formation of the anomalous storm tracks under the influence of SSTA at different scales are discussed in the penultimate section. A summary and discussion of our findings are given in the final section.

Data and methods

The SST data, i.e., data on the initial values and boundaries used in model experiments, are the same as in work (Zhang et al., 2021). The scheme of numerical ensemble experiments is also consistent with work (Zhang et al., 2021). A total of three sets of ensemble numerical experiments with different initial values are designed, and each group has 16 members with different initial values. The integration scheme and the initial and boundary conditions are the same for each group of experiments, but the difference between the three groups of experiments is the different forcing of SSTA. The first group of experiments is called the control test (CTRL), forced by the climatological monthly mean SST [20-year average (1993–2012)] in the North Pacific.

The second set of ensemble experiments uses a KE-related SSTA superimposed on climatological monthly mean SST to force the model, which is called KSTS. This KE-related SSTA is obtained from the monthly mean SSTA regression onto the KE index (KEI) (Qiu and Chen, 2005) in the area (140°E–160°W, 32°N–40°N). The third experiment is mesoscale filtered simulations (MEFS). The 2-D spatial Loess filter was used to separate mesoscale SST from KE-related SSTAs, and the remaining large-scale SSTAs were superimposed on the

climatological monthly mean SST as the boundary SST condition in MEFS. The initial conditions for 16 members are those of September 1 of the different years 1981, 1982, 1985, 1986, 1989, 1990, 1997, 1998, 2000, 2001, 2002, 2003, 2004, 2005, 2006, and 2007. The lateral boundary conditions were climatological (1981–2010) 6 h NCEP2 reanalysis data. The three sets of ensemble experiments were integrated from September 1 to February 2 of the following year, and the first month was the spin-up time. The results of differences between the two groups represent different meanings. KSTS-MEFS represents the response of storm track to mesoscale SSTA. MEFS-CTRL represents the response of storm track to large-scale SSTA. The detailed design of the numerical experiments scheme and the significance test method are drawn from those of Zhang et al. (2021). The storm tracks are represented by the variance or covariance of synoptic disturbances (Chang et al., 2002). Specifically, we chose the variance of synoptic-scale meridional wind velocity ($v'v'$) at 250 hPa and the synoptic-scale transient eddy meridional heat flux $v'T'$ at 850 hPa. The prime stands for the 2–8-day Lancozs bandpass filter. In addition, the cold season refers to the average from October to January in the following year.

Evaluation of model performance in reproducing atmospheric responses to the KE dynamic state changes

The storm tracks of $v'v'$ are significantly strengthened in the central-eastern Pacific Ocean (Figure 1), consistent with the results of previous work (Peng and Whitaker 1999; Liu and Wu 2004; Révelard et al., 2016, Révelard et al., 2018). RegCM4.6 well simulates the response of storm tracks to KE-related SSTAs. We also assessed the ability of the model to simulate atmospheric response to mesoscale SSTAs. Observational studies show that the surface wind speed usually increase over warm eddies and decreases over cold eddies (Chelton et al., 2004, 2007; Bryan et al., 2010), and the boundary layer is also higher over warm eddies and lower over cold eddies (Ma et al., 2015). The response of the boundary layer to the KE-related mesoscale SSTAs is shown in Figure 2. We followed the Holtslag planetary boundary-layer scheme to calculate the height of the boundary layer (Holtslag et al., 1990). The 10 m winds strengthen (weaken) and the boundary-layer height increases (decreases) over the warm (cold) mesoscale SSTAs. This indicates that RegCM4.6 can reproduce the atmospheric boundary-layer response to the KE-related mesoscale SSTA field.

Response of the storm tracks to KE-related large-scale and mesoscale SSTAs

The intensity and location of the storm tracks under the influence of KE-related SSTAs at different scales are shown in Figures 3A,B. KE-related mesoscale SSTAs significantly

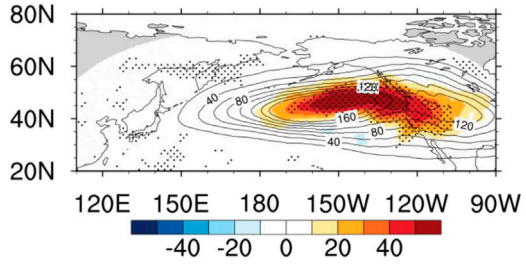

FIGURE 1
250 hPa storm track response to KE-related SSTAs (m^2 s^{-2}, shading). The isoline is the climatological storm track simulated by the model (CTRL). Statistically significant differences at 90% according to Student's *t* test are stippled.

strengthen the storm tracks over the central-eastern Pacific and Gulf of Alaska, while KE-related large-scale SSTAs significantly enhance storm track activity over the eastern North Pacific and near the west coast of the North American continent. Compared with the storm tracks influenced by the large-scale SSTAs, the storm tracks influenced by the mesoscale SSTAs are located slightly northward, as shown in Figure 3C.

The 850 hPa synoptic meridional heat flux $v't'$ was calculated as shown in Figure 4. Under the influence of large-scale SSTAs, there is strong enhancement near 45°N over the central Pacific, while under the influence of mesoscale SSTAs, there is strong enhancement in the area north of 45°N, and its distribution is more northward than that influenced by large-scale SSTAs. The difference between them presents a dipole structure as shown in Figure 4C.

The activity of the storm tracks plays an important role in modulating precipitation at middle and high latitudes (Adler, et al., 2003; Hawkroft et al., 2015). Therefore, the anomalous storm tracks' activity is usually accompanied by precipitation anomalies. As shown in Figure 5, under the influence of KE-related mesoscale SSTAs, there is a positive precipitation anomaly over the central-eastern Pacific Ocean, Gulf of Alaska, and west coast of North America north of 45°N where the storm tracks are active. This conclusion is similar to that of Liu et al. (2021), and their results indicate that the mesoscale SSTAs can exert a remote influence on a landfalling AR (Atmospheric River) on the sub-seasonal to seasonal time scales and related heavy precipitation along the west coast of North America. By contrast, under the influence of KE-related large-scale SSTAs (Figure 5B), there is a heavy precipitation anomaly over the KE large-scale warm SSTAs.

In addition, we compare the precipitation under the influence of KE-related large-scale SSTAs and mesoscale SSTAs, and we find that most of the precipitation in KE area is caused by KE-related large-scale SSTAs, and KE-related mesoscale SSTAs do not cause too much precipitation in KE region. Although mesoscale SSTAs only increase the precipitable water in the atmosphere (Jia et al., 2019), they enhance the precipitation along the North American continental coast far away from KE region. This requires further study on the response of the storm track and precipitation to the scale-dependence of SSTAs.

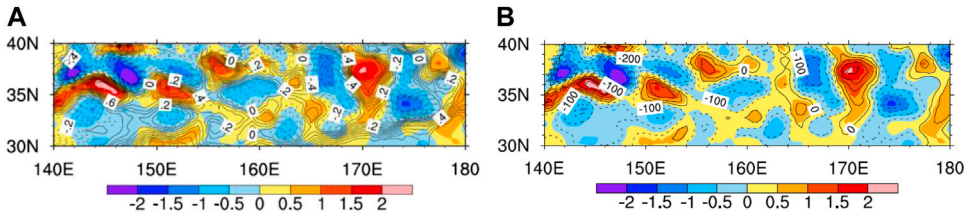

FIGURE 2
Boundary-layer response to KE-related SSTAs in the cold season (KSTS-MEFS). **(A)** KE-related mesoscale SSTAs (°C, shading) and 10 m wind speed (m s^{-1}, contours); **(B)** KE-related mesoscale SSTAs (°C, shading) and boundary-layer thickness anomalies (m, contours).

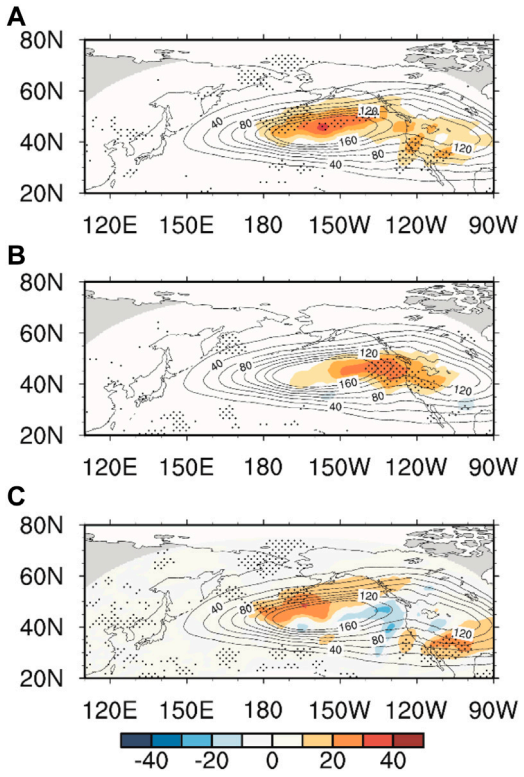

FIGURE 3
Response of storm tracks (m^2 s^{-2}, shading) at 250 hPa to different scales of KE-related SSTAs in KE in the cold season: **(A)** KE-related mesoscale SSTAs (KSTS-MEFS) and **(B)** KE-related large-scale SSTA background (MEFS-CTRL). **(C)** Differences in the response of storm tracks to KE-related mesoscale SSTAs and the response of storm tracks to KE-related large-scale SSTAs. The isoline is the climatological storm track simulated by the model (CTRL). Statistically significant differences at 90% according to Student's *t* test are stippled.

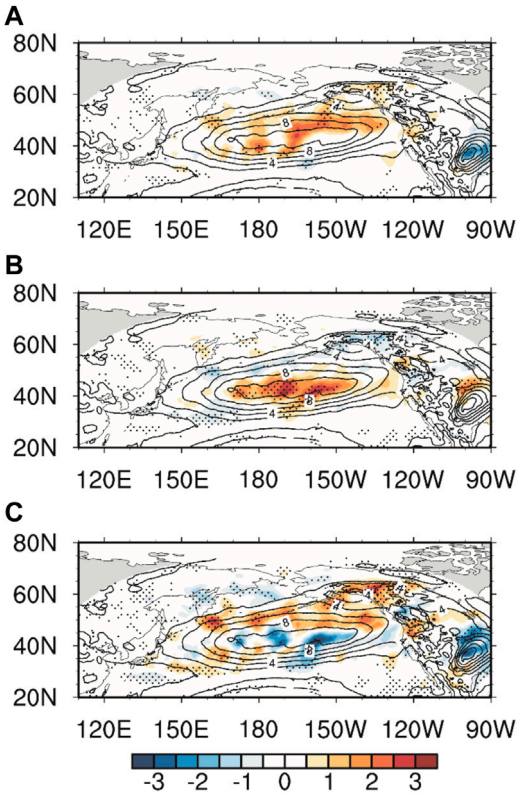

FIGURE 4
Numerical simulations of 850 hPa meridional transient eddy heat flux (K m s^{-1}, shading) in the cold season. **(A)** Response of 850 hPa meridional eddy heat flux to KE-related mesoscale SSTAs (KSTS-MEFS). **(B)** The same as **(A)** but for KE-related large-scale SSTAs (MEFS-CTRL). **(C)** The differences in the response of transient eddy heat flux to KE-related mesoscale SSTAs and the response of transient eddy heat flux to KE-related large-scale SSTAs. The isoline is the climatological meridional transient eddy heat flux simulated by the model (CTRL). Statistically significant differences at 90% according to Student's *t* test are stippled.

Possible mechanism for responses of storm tracks

The baroclinic structure in the lower atmosphere has an important influence on the baroclinic growth of synoptic-scale eddies. The growth rate is usually indicated by the maximum Eady growth rate σ (Lindzen and Farrel 1980):

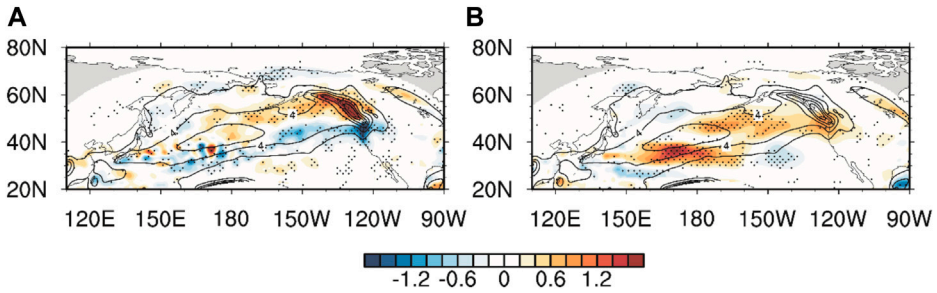

FIGURE 5
Winter mean precipitation (10^{-4} kg m^{-2} s^{-1}, shading) for **(A)** KE-related mesoscale SSTAs (KSTS-MEFS) and **(B)** KE-related large-scale SSTAs (MEFS-CTRL). The isoline is the climatological precipitation simulated by the model (CTRL). Statistically significant differences at 90% according to Student's *t* test are stippled.

$$\sigma = 0.31 \frac{g}{N\theta}\left|\frac{\partial\theta}{\partial y}\right| \quad (1)$$

where N is the Brunt-Väisälä frequency and θ is the potential temperature. A KE-related mesoscale SSTA field leads to strengthened atmospheric baroclinicity over the north of the KE jet axis and the central-eastern North Pacific. We find that atmospheric baroclinicity at 850 hPa caused by KE-related mesoscale SSTAs is significantly enhanced in the western Pacific Ocean north of 40°N and in the central-eastern Pacific Ocean north of 50°N, as shown in Figure 6A. The baroclinicity at 850 hPa is significantly enhanced in the central-eastern Pacific between 40°N and 50°N under the influence of large-scale SSTAs, as shown in Figure 6D. We further decomposed the atmospheric baroclinicity response into the changes caused by atmospheric static stability N and the meridional gradient of potential temperature (Gan 2014), as shown in Eq. (2)

$$\sigma \approx \underbrace{0.31g\Delta\left(N^{-1}\right)\theta^{-1}\left|\partial\theta/\partial y\right|}_{(a)} + \underbrace{0.31gN^{-1}\Delta\left(\theta^{-1}\left|\partial\theta/\partial y\right|\right)}_{(b)} \quad (2)$$

As shown in Figure 6, under the influence of KE-related mesoscale SSTAs, baroclinicity is mainly caused by changes in the meridional gradient of potential temperature (Figure 6B). Under the influence of KE-related large-scale SSTAs, the enhancement of baroclinicity is also mainly caused by the increased meridional gradient of potential temperature (Figure 6E). According to Tao et al. (2019) and Zhang et al. (2020), this change in potential temperature can be explained as the surface heat flux forcing induced by the KE-induced SSTAs. SSTAs can effectively maintain atmospheric baroclinicity through a significant meridional difference in heat flux in the lower atmosphere (Nakamura et al., 2004; Nakamura et al., 2008; Yao et al., 2016). Therefore, we studied the difference in heat flux in the lower atmosphere under the influence of different scales of SSTAs. As shown in Figure 7, the turbulent heat flux (latent heat flux and sensible heat flux, THF) in the lower atmosphere caused by mesoscale SSTAs is well matched with the SSTAs. The THF above the warm mesoscale eddy is stronger, while that above the cold mesoscale eddy is weak. Large-scale SSTAs can cause strong THF in the central Pacific Ocean, and there is a maximum value of the meridional gradient near 40°N, which is larger than that caused by mesoscale SSTAs. It should be noted that this large-scale SSTA warming is accompanied by the stable period of KE. SSTAs (especially at the basin scale) can be forced by atmospheric circulation anomalies, while many data analyses in recent decades have examined the impact of the SST changes in the KE region on the atmospheric circulation across the mid-latitude North Pacific basin (Qiu et al., 2007; Frankignpul et al., 2011; Taguchi et al., 2012; Smirnov et al., 2015; Qiu et al., 2017). A consistent feature resulting from these analyses is that when the KE dynamic state is stable, increased surface turbulent (i.e., sensible + latent) heat fluxes tend to be emitted from ocean to atmosphere. Additionally, we do not find that the baroclinicity region is accompanied by the enhancement of THF under the influence of mesoscale SSTAs, so we need to further explore the possible reasons for the enhancement of atmospheric baroclinicity under the influence of mesoscale SSTAs.

The atmospheric response to low-level thermal anomalies usually shows a zonal movement of baroclinicity, the jet stream, and storm tracks (Chen and Zurita-Gotor, 2008; Nie et al., 2016). This process includes two mechanisms: one is the direct thermal wind response, and the other is indirect transient eddy feedback (Deser et al., 2004; Liu and Wu, 2004). Generally, the convergence of a transient eddy momentum flux acts to strengthen the upper-tropospheric jet, while transient eddy heat flux acts to relax the lower tropospheric baroclinicity, corresponding to a strengthened low-level jet. Meanwhile, the feedback of a transient eddy can cause a latitudinal shift of the lower-level baroclinicity which is responsible for the latitudinal shift of the jet and storm track (Zhang et al., 2012; Nie et al., 2013). Under the influence of mesoscale SSTAs, the northward shift of intensified storm track and baroclinicity may be the feedback of transient eddy (Vallis, 2006), an obvious counterclockwise circulation anomaly, driven by a transient eddy (Zhang et al., 2021), similar to the eddy-driven Ferrel Cell, which can demonstrate this result.

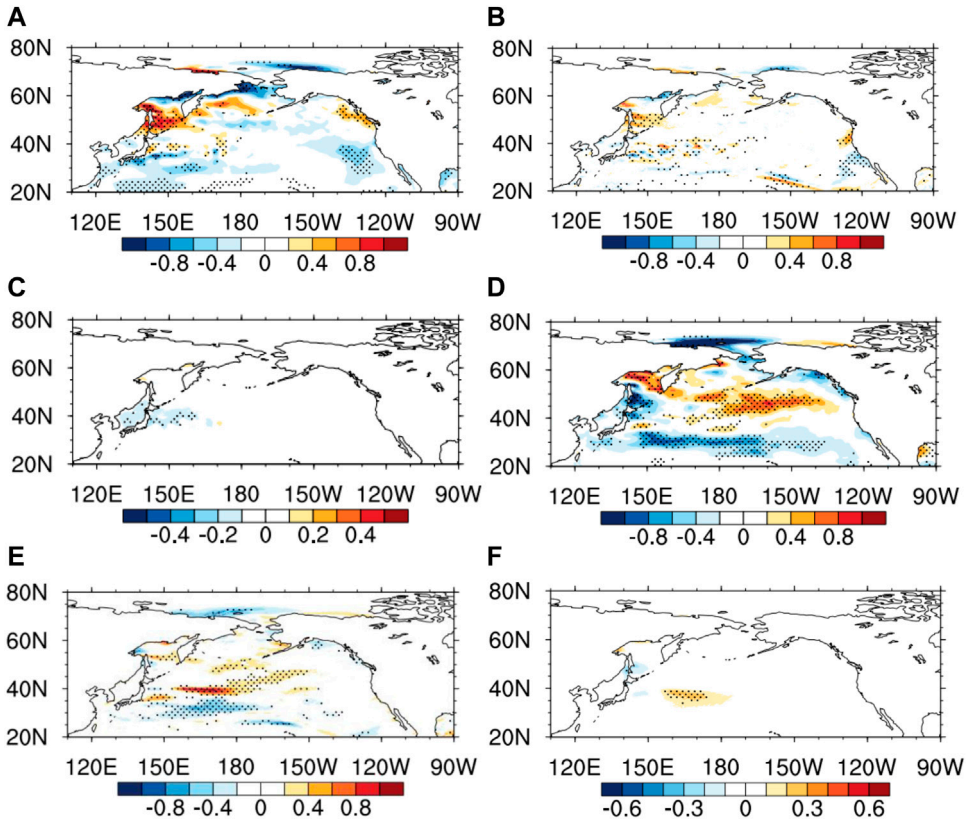

FIGURE 6
Baroclinic growth rate anomaly (10^{-6} s^{-1}, shading) to different scales of KE-related SSTAs at 700 hPa: **(A)** Baroclinicity growth rate in response to KE-related mesoscale SSTAs (KSTS-MEFS). **(B)** Baroclinicity caused by meridional gradient of potential temperature in response to KE-related mesoscale SSTAs (KSTS-MEFS). **(C)** Baroclinicity caused by atmospheric static stability N in response to KE-related mesoscale SSTAs (KSTS-MEFS). **(D–F)** The same as **(A–C)** but for KE-related large-scale SSTAs (MEFS–CTRL). Statistically significant differences at 90% according to Student's *t* test are stippled.

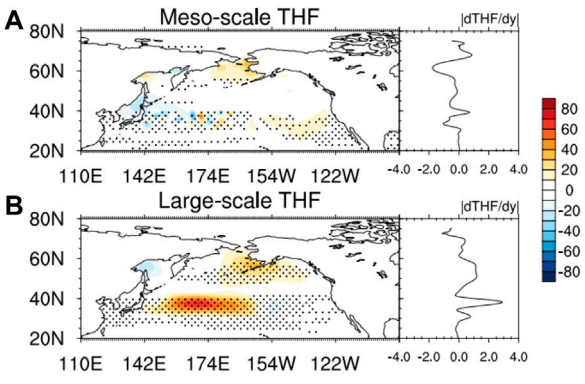

FIGURE 7
Response of surface turbulent heat flux (sensible heat flux and latent heat flux, unit: W m^{-2}) and the average meridional gradient (unit: W m^{-2} (30 km)$^{-1}$) in the interval (150°E~160°W) to different scales of KE-related SSTAs. **(A)** is turbulent heat flux caused by mesoscale SST anomalies, and **(B)** is turbulent heat flux caused by large-scale SST anomalies. Statistically significant differences at 90% according to Student's *t* test are stippled.

We speculate that KE-related mesoscale SSTAs can contribute more to the enhancement of transient eddies, while large-scale warm SSTAs cause more diabatic heating in the central North Pacific, affecting atmospheric circulation, as has been proved by diagnosis in work (Zhang et al., 2021). When transient eddy feedback plays a major role, it can cause the polar movement of baroclinicity and the enhancement of storm tracks. When diabatic heating plays a major role, baroclinicity is maintained to a greater degree by the direct role of thermal wind. Different characteristics of secondary circulation in latitude–altitude sections may be accompanied by different low-level cold and warm temperature advections, which may be the main factor in maintaining baroclinicity (Sun et al., 2018). We calculated horizontal temperature advections under the influence of different scales of KE-related SSTAs, as shown in Figure 8. We found that the influence of mesoscale SSTAs leads to significant warm temperature advections in the western Pacific north of 40°N and in the central-eastern Pacific Ocean north of 50°N. This

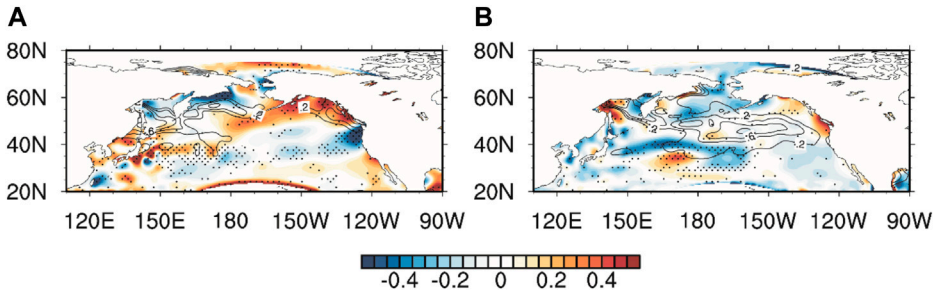

FIGURE 8
Response of air temperature advection at 850 hPa to different scales of KE-related SSTAs (shading, unit: 10^{-3} K s^{-1}), where the isoline is the corresponding atmospheric baroclinicity at 850 hPa (isoline, unit: 10^{-6} s^{-1}), showing only the positive value. **(A)** Response of temperature advection and atmospheric baroclinicity to mesoscale SSTAs; **(B)** response of temperature advection and atmospheric baroclinicity to large-scale SSTAs. Statistically significant differences at 90% according to Student's *t* test are stippled.

enhances the meridional temperature gradient in the north of warm advections and maintains baroclinicity. Under the influence of large-scale SSTAs, we find that there are significant cold temperature advections at approximately 40°N and north of 50°N. It can be found that this baroclinicity affected by temperature advection is mainly reflected in the eastern North Pacific east of 170°W.

There are several factors that affect the efficiency of energy absorption by synoptic transient eddies. According to Cai et al. (2007), these factors include the barotropic energy conversion (BTEC) from mean flow kinetic energy (MKE) to eddy kinetic energy (EKE) and baroclinic energy conversion terms from the mean available potential energy (MAPE) to eddy available potential energy (EAPE) (BCEC1). The energy conversion terms can be expressed as follows:

$$BTEC = \frac{p_0}{g}\left\{\frac{1}{2}\left(\overline{v'^2} - \overline{u'^2}\right)\left(\frac{\partial \bar{u}}{\partial x} - \frac{\partial \bar{v}}{\partial y}\right) - \overline{u'v'}\left(\frac{\partial \bar{v}}{\partial x} + \frac{\partial \bar{u}}{\partial y}\right)\right\} \quad (3)$$

$$BCEC1 = -C_2\left(\overline{u'T'}\frac{\partial \bar{T}}{\partial x} + \overline{v'T'}\frac{\partial \bar{T}}{\partial y}\right) \quad (4)$$

where $C_2 = C_1 (P_0/P)^{R/C_p}/(-d\theta/dp)$, $C_1 = (P_0/P)^{C_v/C_p} R/g$, θ is the potential temperature, g is gravitational acceleration, P_0 is 1000 hPa, R is the dry-air-specific gas constant, and C_v and C_p are the heat capacities at constant pressure and volume, respectively. The primes denote the synoptic transient disturbances, and the overbars represent averaging over the individual cold season months. The energy conversion terms under the influences of KE-related large-scale and mesoscale SSTAs are shown in Figure 9. Here, we calculated the barotropic energy conversion BTEC at 250 hPa in the upper troposphere and BCEC1 at 850 hPa in the lower troposphere. The barotropic energy conversion is weak in the lower troposphere which is not consistent with the storm track in the lower troposphere, so we ignored the contribution of the barotropic energy conversion in the lower troposphere to the storm track. However, the conversion of barotropic energy mainly exists in the upper troposphere because low-frequency energy can be converted to high-frequency energy at the exit of a climatological low-frequency westerly jet stream. As shown in Figure 9A, under the influence of the KE-related mesoscale SSTAs, there are positive BTECs near 50°N located on the left side of westerly jet stream exit, which is beneficial to the strengthening of the storm track. However, under the influence of large-scale SSTAs, as shown in Figure 9B, there are positive BTECs on the right side of the westerly jet stream exit near 40°N, which is conducive to the strengthening of the storm track. BTEC contributes to the storm track of 250 hPa in the upper troposphere. Under the influence of KE-related mesoscale SSTAs, there are strong BCEC1s in the central Pacific and north of approximately 40°N. The enhancement of BCEC1 is beneficial to the transformation of more energy into the available eddy potential energy, which shows good correspondence with the synoptic meridional heat flux at 850 hPa. Under the influence of large-scale SSTAs, BCEC1 is significantly enhanced near 40°N in the central Pacific Ocean, but seems to be limited to approximately 40°N and significantly enhance the synoptic heat flux only near 40°N in the central Pacific Ocean. From the results above, we can argue that the baroclinicity and BCEC play a key role in modulating the storm track response to mesoscale SSTAs and large-scale SSTAs.

Summary and discussion

In this study, we investigate the responses of differential North Pacific storm tracks to multiscale KE-related SSTAs. Different scales of KE-related SSTAs resulted in different locations and intensities of the storm tracks. KE-related mesoscale SSTAs usually led to significant enhancement of the storm tracks in the central-eastern Pacific and Gulf of Alaska north of 40°N, while KE-related large-scale SSTAs led

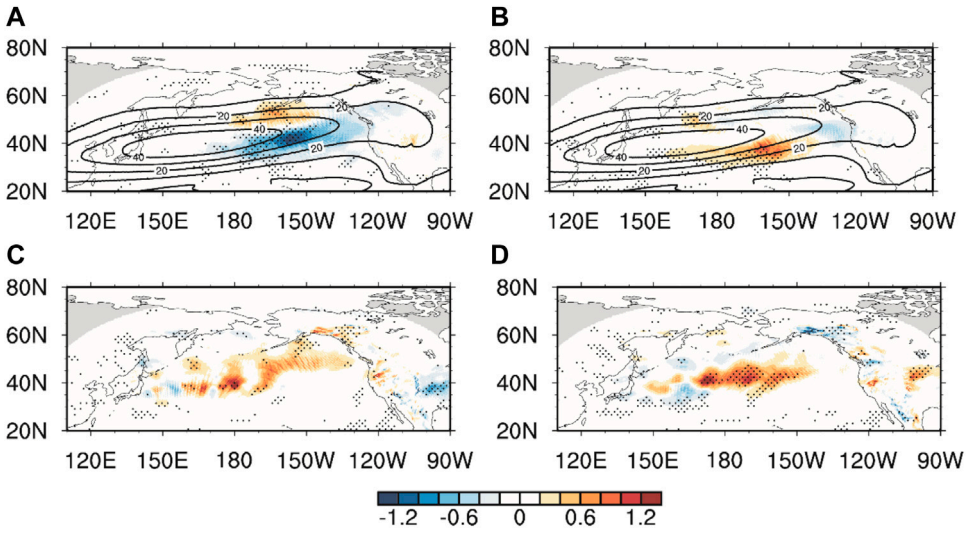

FIGURE 9
Response of energy conversion terms to **(A,B)** KE-related mesoscale SSTAs (KSTS-MEFS) and **(C,D)** KE-related large-scale SSTAs (MEFS-CTRL) at 850 hPa. **(A,C)** Energy conversion from mean available potential energy to eddy available potential energy (BCEC1, W m^{-2}, shading). **(B,D)** Energy conversion from eddy available potential energy to eddy kinetic energy (BCEC2, W m^{-2}, shading). Statistically significant differences at 90% according to Student's *t* test are stippled.

to significant enhancement of the storm tracks over the central Pacific and near the west coast of the North American continent. Under the influence of different scales of KE-related SSTAs, precipitation also shows some differences. Although some studies show that mesoscale SSTAs enhances atmospheric precipitable water (Jia et al., 2019; Zhou and Cheng, 2022; Liu et al., 2021), a remote impact is also seen on precipitation along west coast of North America continent, which may have some influence on the sub-seasonal to seasonal scale. The large-scale SSTAs directly affect precipitation over the local region, and the scale-dependence of this precipitation still deserves further discussion.

Further analysis of the causes shows that the differences in storm tracks are related to barotropic energy conversion and anomalies of lower-level baroclinicity accompanying the corresponding baroclinic energy conversion. Baroclinicity anomalies are related to changes in potential temperature in meridional gradients under the influences of KE-related large-scale and mesoscale SSTAs. The response of the horizontal warm advection of temperature in the lower atmosphere to mesoscale SSTAs shifts the baroclinicity anomaly northward, while under the influence of large-scale SSTAs, the horizontal cold advection of temperature anomaly in the lower atmosphere strengthens and inhibits the northward movement of baroclinicity in the eastern North Pacific. We also briefly discussed the similarities and differences in the formation of baroclinicity corresponding to storm tracks, which is mainly affected by temperature advection. From the above conclusions, it should be noted that different scales of SSTAs in KE region can contribute some to storm track anomaly and precipitation anomaly, showing the scale-dependence of the atmospheric response to SSTAs, which is worthy of further discussion.

Data availability statement

The original contributions presented in the study are included in the article/supplementary material, further inquiries can be directed to the corresponding author.

Author contributions

CC contributed to the writing of the article. JZ contributed methods and data analysis. XC performed data collation and analysis.

Funding

This research was supported by the National Natural Science Foundation of China (42275169).

Conflict of interest

The authors declare that the research was conducted in the absence of any commercial or financial relationships that could be construed as a potential conflict of interest.

Publisher's note

References

Adler, R. F., Huffman, G. J., Chang, A., Ferraro, R., Ping-Ping, X., John, J., et al. (2003). The version 2 global precipitation climatology project (GPCP) monthly precipitation analysis(1979-present). *J. Hydrometeorol.* 4, 1147–1167. doi:10.1175/1525-7541(2003)004<1147:TVGPCP>2.0.CO;2

Cai, M., Yang, S., Van den Dool, H. M., and Kousky, V. E. (2007). Dynamical implications of the orientation of atmospheric eddies: A local energetics perspective. *Tellus A Dyn. Meteorology Oceanogr.* 59, 127–140. doi:10.1111/j.1600-0870.2006.00213.x

Chang, E. K. M., Lee, S., and Swanson, K. L. (2002). Storm track dynamics. *J. Clim.* 15, 2163–2183. doi:10.1175/1520-0442(2002)015<02163:STD>2.0.CO;2

Chelton, D. B., Schlax, M. G., Freilich, M. H., and Milliff, R. E. (2004). Satellite measurements reveal persistent small-scale features in ocean winds. *Science* 303, 978–983. doi:10.1126/science.1091901

Chelton, D. B., Schlax, M. G., Samelson, R. M., and DeSzoeke, R. A. (2007). Global observations of large oceanic eddies. *Geophys. Res. Lett.* 34. doi:10.1029/2007gl030812

Chen, G., and Zurita-Gotor, P. (2008). The tropospheric jet response to prescribed zonal forcing in an idealized atmospheric model. *J. Atmos. Sci.* 65, 2254–2271. doi:10.1175/2007jas2589.12007JAS2589.1

Deser, C., Magnusdottir, G., Saravanan, R., and Phillips, A. (2004). The effects of North Atlantic SST and sea ice anomalies on the winter circulation in CCM3. Part II: Direct and indirect components of the response. *J. Clim.* 17, 877–889. doi:10.1175/1520-0442(2004)017<0877:TEONAS>2.0.CO;2

Bryan, F. O., Tomas, R., Dennis, J. M., Chelton, D. B., Loeb, N. G., and McClean, J. L. (2010). Frontal scale Air-sea interaction in high-resolution coupled climate models. *J. Clim.* 23, 6277–6291. doi:10.1175/2010jcli3665.1

Foussarde, A., Lapeyre, G., and Plougonven, R. Storm track response to oceanic eddies in idealized atmospheric simulations[J] . *J. Clim.*, 2018, 32: 445–463, doi:10.1175/JCLI-D-18-0415.1

Frankignoul, C., Sennéchael, N., Kwon, Y. O., and Alexander, M. A. (2011). Influence of the meridional shifts of the kuroshio and the oyashio extensions on the atmospheric circulation. *J. Clim.* 24 (3), 762–777. doi:10.1175/2010JCLI3731.1

Gan, B. (2014). *Interaction between wintertime storm tracks and extratropical oceans in the Northern Hemisphere [D]*. Qingdao, China: Ocean University of China.

Hawcroft, M. K., Shaffrey, L. C., Hodges, K. I., and Dacre, H. F. (2015). Can climate models represent the precipitation associated with extratropical cyclones? [j]. *Clim. Dyn.* 47, 679–695. doi:10.1007/s00382-015-2863-z

Holtslag, A. A. M., Bruijn, E. I. F. D., and Pan, H. L. (1990). A high-resolution air-mass transformation model for short-range weather forecasting. *Mon. Weather Rev.* 118 (8), 1561–1575. doi:10.1175/1520-0493(1990)118<1561:AHRAMT>2.0.CO;2

Jia, Y. L., Chang, P., Szunyogh, I., Saravanan, R., and Bacmeister, J. T. (2019). A modeling strategy for the investigation of the effect of mesoscale SST variability on atmospheric dynamics. *Geophys. Res. Lett.* 46, 3982–3989. doi:10.1029/2019GL081960

Kida, S., Mitsudera, H., Aoki, S., Guo, X., Shin-ichi, I., Kobashi, F., et al. (2015). Oceanic fronts and jets around Japan: A review. *J. Oceanogr.* 71(5), 469–497. doi:10.1007/s10872-015-0283-7

Kushnir, Y., Robinson, W. A., Bladé, I., Hall, N. M. J., Peng, S., and Sutton, R. (2002). Atmospheric gcm response to extratropical sst anomalies: Synthesis and evaluation. *J. Clim.* 15 (16), 2233–2256. doi:10.1175/1520-0442(2002)015<2233:AGRTES>2.0.CO;2

Kwon, Y.-O., and Joyce, T. M. (2013). Northern Hemisphere winter atmospheric transient eddy heat fluxes and the Gulf Stream and Kuroshio–Oyashio Extension variability. *J. Clim.* 26, 9839–9859. doi:10.1175/JCLI-D-12-00647.1

Lindzen, R. S., and Farrell, B. (1980). A simple approximate result for the maximum growth rate of baroclinic instabilities. *J. Atmos. Sci.* 37 (7), 1648–1654. doi:10.1175/1520-0469(1980)037<1648:asarft>2.0.co;2

Liu, X., Ma, X., Chang, P., Jia, Y., Fu, D., Xu, G., et al. (2021). Ocean fronts and eddies force atmospheric rivers and heavy precipitation in Western North America. *Nat. Commun.* 12, 1268. doi:10.1038/s41467-021-21504-w

Liu, Z., and Wu, L. (2004). Atmospheric response to north pacific SST: The role ofOcean–atmosphere coupling*. *J. Clim.* 17, 1859–1882. doi:10.1175/1520-0442(2004)017<1859:artnps>2.0.co;2

Ma, X. H., Chang, P., Saravanan, R., Montuoro, R., Hsieh, J-S., Wu, D. X., et al. (2015). Distant influence of Kuroshio eddies on north Pacific weather patterns? *Sci. Rep.* 5, 17785. doi:10.1038/srep17785

Nakamura, H., Sampe, T., Goto, A., Ohfuchi, W, and Xie, S. On the importance of midlatitude oceanic frontal zones for the mean state and dominant variability in the tropospheric circulation[J]. *Geophysical Research Letters*, 2008, 35(15):971–978.

Nakamura, H., Sampe, T., Tanimoto, Y., and Shimpo, A. (2004). "Observed associations among storm tracks, jet streams and midlatitude oceanic fronts," in *Earth's climate: The ocean-atmosphere interaction*. *Geophys. Monogr.* Editors C. Wang, S.-P. Xie, and J. A. Carton (Washington, D.C., U.S.A.: American Geophysical Union), 147, 329–346.

Nie, Y., Zhang, Y., Yang, X.-Q., and Chen, G. (2013). Baroclinic anomalies associated with the Southern Hemisphere annular mode: Roles of synoptic and low-frequency eddies. *Geophys. Res. Lett.* 40, 2361–2366. doi:10.1002/grl.50396

Nie, Y., Zhang, Y., Chen, G., and Yang, X. Q. (2016). Delineating the barotropic and baroclinic mechanisms in the midlatitude eddy-driven jet response to lower-tropospheric thermal forcing. *J. Atmos. Sci.* 73 (1), 429–448. doi:10.1175/jas-d-15-0090.1

Okajima, S, Nakamura, H, Nishii, K., Miyasaka, T., Kuwano-Yoshida, A., Taguchi, B., et al. (2018). Mechanisms for the maintenance of the wintertime basin-scale Atmospheric response to decadal SST variability in the north pacific subarctic frontal zone. *Journal of Climate* 31, 297–315. doi:10.1175/jcli-d-17-0200.1

Peng, S., and Whitaker, J. S. (1999). Mechanism determining the atmospheric response to Midlatitude SST Anomalies. *Journal of Climate* 12, 1393–1408. doi:10.1175/1520-0442(1999)012<1393:MDTART>2.0.CO;2

Qiu, B., Chen, S., Schneider, N., and Taguchi, B. (2014). A coupled decadal prediction of the dynamic state of the kuroshio extension system. *J. Clim.* 27, 1751–1764. doi:10.1175/jcli-d-13-00318.1

Qiu, B., Chen, S., and Schneider, N. (2017). Dynamical links between the decadal variability of the oyashio and kuroshio extensions. *J. Climate* 30, 9591–9605. doi:10.1175/jcli-d-17-0397.1

Qiu, B., and Chen, S. (2005). Variability of the Kuroshio Extension jet, recirculation gyre and mesoscale eddies on decadal timescales. *Journal of Physical Oceanography* 35, 2090–2103. doi:10.1175/JPO2807.1

Qiu, B. (2000). Interannual variability of the kuroshio extension system and its impact on the wintertime sst field. *J. Phys. Oceanogr.* 30 (6), 1486–1502. doi:10.1175/1520-0485(2000)030<1486:ivotke>2.0.co;2

Qiu, B., Schneider, N., and Chen, S. (2007). Coupled decadal variability in the North Pacific: An observationally-constrained idealized model. *J. Clim.* 20, 3602–3620. doi:10.1175/jcli4190.1

Révelard, A., Frankignoul, C., and Kwon, Y-O. (2018). A multivariate estimate of the cold season atmospheric response to north pacific SST variability. *J. Clim.* 31, 2771–2796. doi:10.1175/JCLI-D-17-0061.1

Révelard, A., Frankignoul, C., Sennéchael, N., Kwon, Y.-O., and Qiu, B. (2016). Influence of the decadal variability of the Kuroshio Extension on the atmospheric circulation in the cold season. *J. Clim.* 29, 2123–2144. doi:10.1175/JCLI-D-15-0511.1

Smirnov, D., Newman, M., Alexander, M. A., Kwon, Y.-O., and Frankignoul, C. (2015). Investigating the local atmospheric response to a realistic shift in the Oyashio sea surface temperature front. *J. Clim.* 28, 1126–1147. doi:10.1175/jcli-d-14-00285.1

Sun, X., Tao, L., and Yang, X.-Q. (2018). The influence of oceanic stochastic forcing on the atmospheric response to midlatitude North Pacific SST anomalies. *Geophys. Res. Lett.* 45 (17), 9297–9304. doi:10.1029/2018gl078860

Taguchi, B., Nakamura, H., Nonaka, M., Komori, N., Kuwano-Yoshida, A., Takaya, K., et al. (2012). Seasonal evolutions of atmospheric response to decadal sst anomalies in the North Pacific subarctic frontal zone: Observations and a coupled model simulation. *Journal of Climate* 25 (1), 111–139. doi:10.1175/jcli-d-11-00046.1

Taguchi, B., Nakamura, H., Nonaka, M., and Xie, S. P. (2009). Influences of the kuroshio/oyashio extensions on air–sea heat exchanges and storm-track activity as revealed in regional atmospheric model simulations for the 2003/04 cold season. *Journal of Climate* 22 (24), 6536–6560. doi:10.1175/2009jcli2910.1

Tanimoto, Y., Nakamura, H., Kagimoto, T., and Yamane, S. (2003). An active role of extratropical sea surface temperature anomalies in determining anomalous turbulent heat flux. *J. Geophys. Res.* 108 (C10), 3304. doi:10.1029/2002jc001750

Tao, L. F., Sun, X. G., and Yang, X.-Q. (2019). The asymmetric atmospheric response to the midlatitude North pacific SST anomalies. *J. Geophys. Res. Atmos.* 124 (16), 9222–9240. doi:10.1029/2019JD030500

Vallis, G. K. (2006). in *Atmospheric and ocean fluid dynamics: Fundamentals and large-scale circulation*. Editor G. K. Vallis (Cambridge, UK: Cambridge University Press), 770. doi:10.1017/CBO9780511790447

Vivier, F., Kelly, K. A., and Thompson, L. (2002). Heat budget in the kuroshio extension region: 1993–99. *J. Phys. Oceanogr.* 32 (12), 3436–3454. doi:10.1175/1520-0485(2002)032<3436:hbitke>2.0.co;2

Wang, Y-H., and Liu, W. T. (2015). Observational evidence of frontal-scale Atmospheric responses to kuroshio extension variability. *J. Clim.* 28, 9459–9472. doi:10.1175/jcli-d-14-00829.1

Yao, Y., Zhong, Z., and Yang, X-Q. (2016). Numerical experiments of the storm track sensitivity to oceanic frontal strength within the Kuroshio/Oyashio Extensions. *J. Geophys. Res. Atmos.* 121, 2888–2900. doi:10.1002/2015JD024381

Zhang, C., Liu, H., Xie, J., Lin, P., Song, J., Yang, Q., et al. (2020). North Pacific storm track response to the mesoscale sst in a global high-resolution atmospheric model. *Clim. Dyn.* 55, 1597–1611. doi:10.1007/s00382-020-05343-x

Zhang, J., Li, C., and Zhang, C. (2021). Response of atmospheric circulation to multiscale sst anomaly associated with kuroshio extension decadal variability warming in winter. *Sci. China Earth Sci.* 64 (12), 2098–2112. doi:10.1007/s11430-020-9831-3

Zhang, Y., Yang, X., Nie, Y., and Chen, G. (2012). Annular mode–like variation in a multilayer quasigeostrophic model. *J. Atmos. Sci.* 69, 2940–2958. doi:10.1175/jas-d-11-0214.1

Zhou, G. D., and Cheng, X. H. (2022). Impacts of oceanic fronts and eddies in the Kuroshio-Oyashio Extension region on the atmospheric general circulation and storm track. *Adv. Atmos. Sci.* 39 (1), 22–54. doi:10.1007/s00376-021-0408-4